Journal of Crystal Growth 375 (2013) 119–124

Contents lists available at SciVerse ScienceDirect

Journal of Crystal Growth

journal homepage: www.elsevier.com/locate/jcrysgro

Pholcodine monohydrate: Crystal structure and polymorphism

Gjorgji Petruševski [a,*], Marija Zbačnik [b], Marina Kajdžanoska [a], Sonja Ugarkovic [a], Vase Trimčeski [c], Branko Kaitner [b], Gligor Jovanovski [d,e], Petre Makreski [e]

[a] Research & Development, ALKALOID AD, Aleksandar Makedonski 12, 1000 Skopje, Republic of Macedonia
[b] Laboratory of General and Inorganic Chemistry, Department of Chemistry, Faculty of Science, University of Zagreb, Horvatovac 102a, 10002 Zagreb, Croatia
[c] Production of pharmaceutical raw materials, Partizanski odredi 98 A, ALKALOID AD, 1000 Skopje, Republic of Macedonia
[d] Macedonian Academy of Sciences and Arts, Krste Misirkov 2, 1000 Skopje, Republic of Macedonia
[e] Institute of Chemistry, Faculty of Science, SS. Cyril and Methodius University, Arhimedova 5, 1000 Skopje, Republic of Macedonia

ARTICLE INFO

Article history:
Received 20 February 2013
Received in revised form
8 April 2013
Accepted 11 April 2013
Communicated By: S.R. Qiu
Available online 19 April 2013

Keywords:
A1. Crystal structure
A1. Polymorphism
A1. Recrystallization
A1. X-ray diffraction
B2. Pharmaceuticals

ABSTRACT

The first crystal structure elucidation of pholcodine monohydrate, an important antitussive active pharmaceutical ingredient is reported herein. The studied compound crystallizes in the orthorhombic system in the space group $P2_12_12_1$. Each H_2O molecule is shared by two pholcodine molecules *via* three strong hydrogen bonds. The detailed crystallization screening from several different organic solvents afforded single crystals with various quality, all exhibiting prism-to-needlelike micro morphology. The investigation of the obtained single crystals by means of several physico-chemical, solid-state instrumental techniques (FT-IR, DSC, TG/DTG and XRPD) proved that pholcodine monohydrate exists in a single crystalline modification, identical to the commercial form of the compound.

1. Introduction

Pholcodine monohydrate (7,8-didehydro-4,5α-epoxy-17-methyl-3-[2 (morpholin-4-yl)ethoxy]morphinan-6α-ol monohydrate) (Fig. 1) is a semisynthetic morphine derivative extensively used worldwide as antitussive active pharmaceutical ingredient (API) [1–3]. The substance is considered generally safer for medical application compared to similar morphine antitussive analogs (e.g. codeine) because it neither causes depression of respiration, nor central nervous system excitation, thus avoiding the risk of euphorizing properties or addiction [3]. Although it has been in active pharmaceutical use since the late 1950s, recently it gained new scientific attention, as the pharmacokinetics and metabolism are not known in detail [2,4,5]. In addition, during the past decade considerable emphasis has been placed on the need to develop and validate suitable high performance liquid chromatography (HPLC) methods for identification and quantification of the bulk API and the corresponding process and degradation impurities [6,7].

Pholcodine monohydrate has seen several decades of intense pharmaceutical/medical application history, but it is peculiar that negligible scientific information were reported concerning its solid-state properties. Moreover, to the best of our knowledge, no results are published related either to pholcodine crystal structure or its polymorphism being unusual, having in mind the well established scientific facts about the possible influences of different polymorphs of a single API toward the physico-chemical properties such as solubility, stability and occasionally even the bioavailability of the corresponding drug product [8–11]. Detailed search in the Cambridge Structural Database (June 2012 version) confirmed that the crystal structure of pholcodine monohydrate (or any other pholcodine derivative) has not been elucidated.

The main scientific goal of the present study is to determine, for the first time, the crystal structure of pholcodine monohydrate and to describe its structural features in detail. The commercial sample of pholcodine monohydrate was crystallized from a series of organic solvents in order to isolate the suitable single crystals for X-ray structure analysis. As the polymorphism and/or solvatomorphism of this compound was not reported in the literature, all crystallized samples were analyzed by means of a combination of several solid-state instrumental techniques, such as: optical microscopy, Fourier transform infrared (FT-IR) spectroscopy, differential scanning calorimetry (DSC), thermogravimetric analysis (TG/DTG) and X-ray powder diffraction (XRPD). The application of such powerful methodology is already proven to be a very fast, precise and reliable research approach for adequate study of polymorphism and/or solvatomorphism in morphine related antitussive API like codeine phosphates analogs [10,11]. Presentation of the obtained data from the solid-state properties screening of pholcodine monohydrate will

* Corresponding author. Tel.: +389 2 3104 115; fax: +389 2 3104 049.
E-mail address: gjpetrusevski@Alkaloid.com.mk (G. Petruševski).

0022-0248/$ - see front matter © 2013 Elsevier B.V. All rights reserved.
http://dx.doi.org/10.1016/j.jcrysgro.2013.04.031

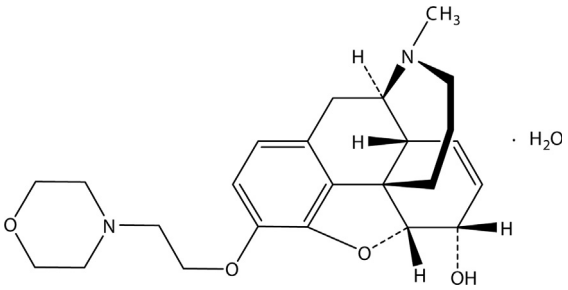

Fig. 1. Structural formula of pholcodine monohydrate.

be also beneficial in the pharmaceutical research and quality control laboratories worldwide.

2. Materials and methods

2.1. Materials

Pholcodine monohydrate, assay: 99.59% by potentiometric titration on dried substance and loss on drying: 4.4% [1], used in this study is a commercial sample of the compound as produced by ALKALOID AD (Macedonia). Methanol, absolute ethanol, acetone, ethyl acetate, tetrahydrofuran (THF) and *N,N*–dimethylformamide (DMF) with *pro analysis* quality were acquired from Merck and used without further purification.

2.2. Crystallization of pholcodine monohydrate

In order to obtain the suitable single crystals of pholcodine monohydrate for X-ray structure analysis, commercial sample of the staring material was crystallized by slow evaporation of hot solutions of the drug in several solvents. Absolute ethanol (water content≤0.1%) and methanol (water content≤0.03%) were selected from the protic class of solvents, acetone (water content≤0.05%) and ethyl acetate (water content≤0.05%) from the Lewis bases class of solvents and tetrahydrofuran (water content≤0.02%) and *N,N*–dimethylformamide (water content≤0.3%) from the dipolar aprotic class of solvents. Saturated solutions of pholcodine monohydrate were obtained by adding the substances in preheated (35 °C) solvent (10 mL) until the undissolved portion was still observable after 10 min of constant mixing using a magnetic stirrer. The saturated solution was quickly filtered into 25 mL crystallization vessels, and the filtrate was left to evaporate at controlled ambient temperature of 23 ± 2 °C under constant laminar air stream. After complete solvent evaporation, the crystallizing vessels were placed under dried silica atmosphere to stabilize 48 h before further analysis.

2.3. Fourier transform infrared (FT-IR) spectroscopy

The FT-IR spectra were recorded on a Varian 660 FT-IR spectrometer using three different sampling protocols. Standard KBr pellets method was applied, collecting the spectra in the 4000–400 cm^{-1} region. FT-IR spectra obtained as Fluorolube (4000–2000 cm^{-1}) and Nujol (2000–550 cm^{-1}) dispersions were recorded using 10–20 mg of samples dispersed manually in two drops of the agent. The prepared dispersion was applied on KBr pellets in a form of thin film and FT-IR transmission spectra were recorded. Attenuated total reflectance (ATR) spectra (4000–550 cm^{-1} region) were obtained by MIRAcle ZnSe ATR module (PIKE technologies) with low pressure micrometer clamp. Corrections of the ATR spectra for the wavenumber-dependent variations in the depth of penetration were undertaken using the in-built ATR correct Algorithm 2 in the Varian Resolutions Pro software [12]. The following settings were introduced in the algorithm menu: crystal angle of incidence (45°), crystal (ZnSe), crystal refractive index (2.403), and sample refractive index (1.5). All spectra were averaged from 32 scans per spectrum and the resolution was set to 4 cm^{-1}.

2.4. Differential scanning calorimetry (DSC) and thermogravimetric analysis (TGA)

DSC measurements were carried out in cyclic mode of operation. The procedure started by heating from 25 °C to 120 °C, cooling to 0 °C and reheating to 120 °C, applying a heating/cooling rate of 5 °C/min. The measurements were carried out under dynamic nitrogen atmosphere (30 mL/min) in pierced aluminum pans with Netzsch DSC 204 F1 *Phoenix* instrument. The TG and DTG curves were recorded in the 30–400 °C range, on a Netzsch TG 209 F1 *Iris* analyzer using ceramic/aluminum sample pans.

2.5. Optical microscopy

Microscopic images were obtained using Malvern-Morphologi G3S particle size and morphology analyzer microscope, coupled with a 5 megapixel CCD camera. The micro-images were obtained using bright field mode at 5, 10 and 20-fold optical magnifications.

2.6. X-ray powder diffraction

The X-ray powder diffraction (XRPD) measurements were conducted on a Rigaku Ultima IV powder X-ray diffractometer. Each studied sample was manually dispersed over a silicon sample plate and the data were collected at room temperature on a D/tex detector in the 2θ range from 3 to 45° (scan rate 2 °/min). CuKα radiation was obtained from a generator set at 40 kV and a current of a 40 mA.

2.7. Single crystal X-ray structure analysis

The molecular and crystal structures of the title compound were determined by single crystal X-ray diffraction. The diffraction data were collected at 120 K (liquid nitrogen). The diffraction measurement was performed on an Oxford Diffraction Xcalibur Kappa CCD X-ray diffractometer using graphite-monochromated MoKα radiation ($\lambda=0.71073$ Å). The data sets were collected using the ω scan mode over the 2θ range to 54°. Programs CrysAlis CCD and CrysAlis RED [13] were used for data collection, cell refinement and data reduction. The structure was solved by direct methods and refined using SHELXS and SHELXL programs, respectively [14]. The structural refinement was performed on F^2 using all data. The hydrogen atoms bound to non-chiral carbon atoms were placed in calculated positions and treated as riding on their parent atoms [C–H=0.93 Å and $U_{iso}(H)=1.2\ U_{eq}(C)$]. The riding mode was dependent on the type of hybridization of the C atom. The hydrogen atoms bound to chiral carbon atoms were located in the difference Fourier map and refined in subsequent refinement cycles. All calculations were performed using the WINGX crystallographic suite of programs [15]. The molecular structure of the compound is presented by ORTEP-3 [16] and POV-RAY [17] programs. The hydrogen bonding projection was prepared using Mercury 2.3 [18]. Hirshfeld surfaces [19] and corresponding fingerprint plots [20] were prepared using CrystalExplorer 2.1. Table. S1 lists the general, single crystal X-ray diffraction and refinement data for the title compound at 120 K.

3. Results and discussion

Crystallization experiments using different solvents afforded crystals of varying quality (Fig. S1). The first crystals appeared in the filtrates of acetone and ethyl acetate solution, 2 h after filtration.

In all other solutions, except DMF, crystals appeared 48 h after filtration and complete evaporation was achieved after 3 or 4 days.

As the DMF solution had not evaporated even after 5 days, it was transferred to a 10 cm Petri dish and heated at 45 °C for 2 h, until complete evaporation of the solvent and deposition of crystal agglomerates (Fig. S1f). The bright field optical microscopic screening afforded initial verification that single crystals, with varying quality are formed in all cases, adopting similar prism-to-needlelike micro morphology.

3.1. Solid-state characterization of the crystallized samples

3.1.1. FT-IR spectroscopy

The FT-IR spectra of the starting material and the crystallized samples collected using KBr pellets and ATR method are presented in Fig. 2. As seen, regardless of the sampling method, the spectral curves appeared practically identical. In addition, the FT-IR spectra (Fig. 2b–g) of the crystallized samples are equal to the spectrum of the commercial pholcodine monohydrate sample (Fig. 2a). In order to exclude even minimal pressure exposure and prevent the possibility for phase transformations or desolvation/dehydration that might occur during the compression steps using KBr pellet or ATR (low pressure micrometer clamp) methods in the sample preparation, FT-IR spectra obtained from Fluorolube (Fig. S2) and Nujol dispersion were also collected (Fig. S3). The obtained data again confirmed unaltered FT-IR patterns for all crystallized samples compared to the corresponding spectrum of the initial commercial sample. Solely in the case of the DMF crystallized sample (Fig. S3g), the spectrum obtained from the material prepared as Nujol disspersion revealed the presence of a small, physically adsorbed quantity of residual DMF (typical DMF carbonyl band observable at about 1660 cm^{-1}).

3.1.2. Differential scanning calorimetry (DSC) and thermogravimetric analysis (TG/DTG)

DSC curves of the commercial pholcodine monohydrate sample and the crystallized samples are presented in Fig. 3. In contrast to the FT-IR spectroscopic findings, where identical spectral pattern were observed in all cases, the DSC curves exhibit significant

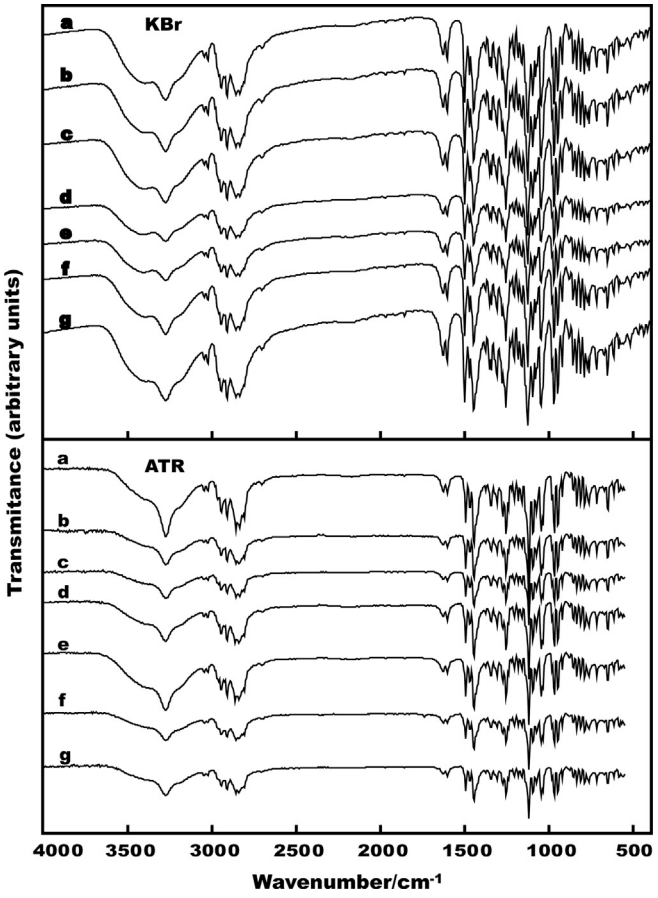

Fig. 2. FT-IR spectra (KBr pellet and ATR) of pholcodine monohydrate commercial sample (a) compared to the corresponding spectra of the crystallized samples from: acetone (b), ethyl acetate (c), methanol (d), ethanol (e), THF (f) and DMF (g).

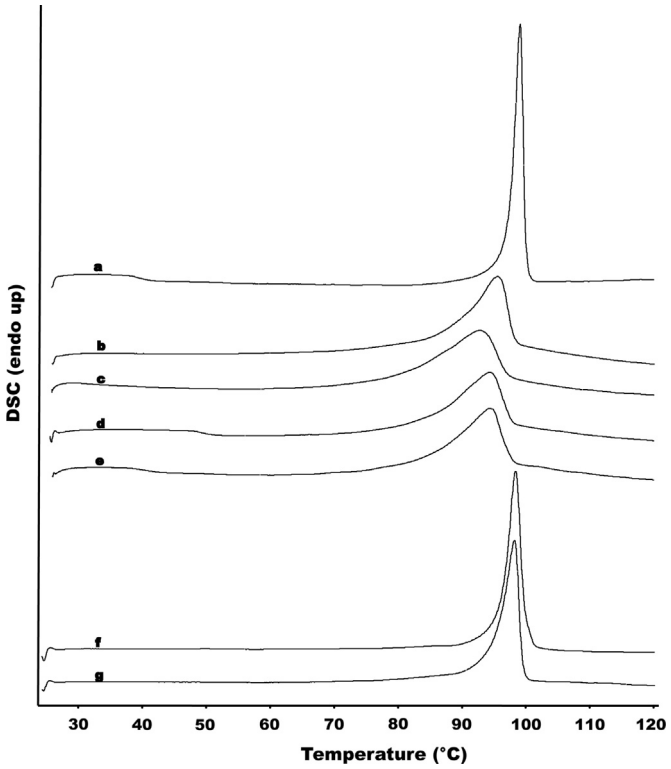

Fig. 3. DSC curves (first heating run) of pholcodine monohydrate commercial sample (a) compared to the corresponding curves for the crystallized samples from: acetone (b), ethyl acetate (c), methanol (d), ethanol (e), THF (f) and DMF (g).

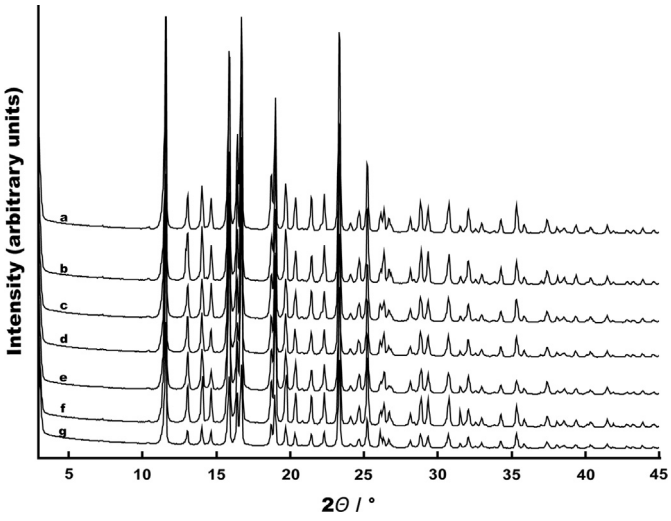

Fig. 4. XRPD patterns of pholcodine monohydrate commercial sample (a) compared to the corresponding patterns obtained for the crystallized samples from: acetone (b), ethyl acetate (c), methanol (d), ethanol (e), THF (f) and DMF (g).

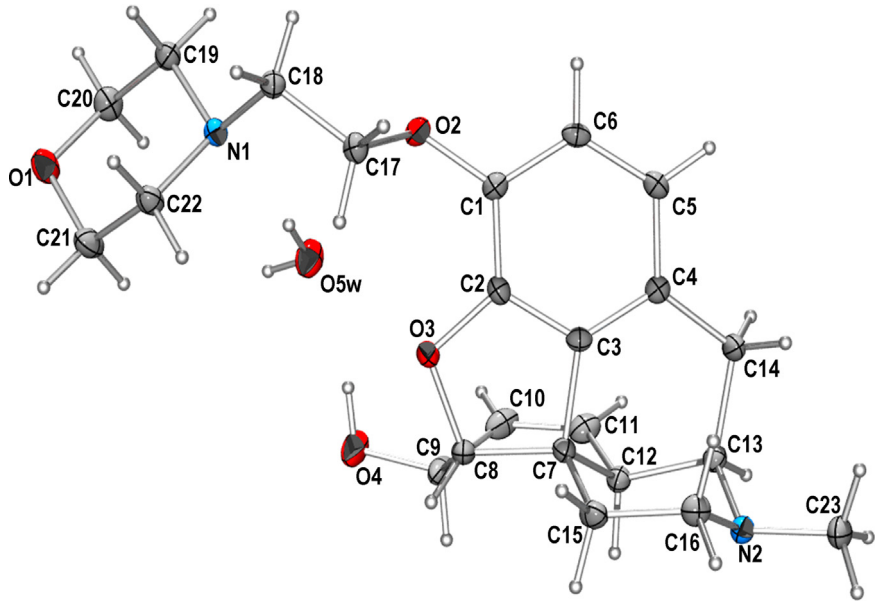

Fig. 5. ORTEP-3 drawing of pholcodine monohydrate showing the crystallographic labeling scheme. Displacement ellipsoids are drawn at the 50% probability level and H atoms are shown as small spheres of arbitrary radius.

Table 1
Hydrogen bond geometry (distances/Å, angles/°).

D–H···A	D–H	H···A	D···A	D–H···A
O5w–H51w···N1	0.868(2)	2.249(2)	3.108(1)	170(2)
O4–H4···O5w	0.862(2)	1.910(2)	2.745(1)	163(2)
O5w–H52w···N2^{i}	0.892(2)	2.029(2)	2.897(1)	164(2)
C8–H8···O1^{ii}	0.980	2.627	3.459	134.8
C19–H19B···O2^{iii}	0.970	2.936	3.424	112.3
C20–H20A···O2^{iii}	0.970	2.791	3.496	130.2

Symmetry codes: (i) $-x+2, y-1/2$; (ii) $-x+1, y+1/2, -z+1/2$; (iii) $x-1/2, -y+1/2, -z$.

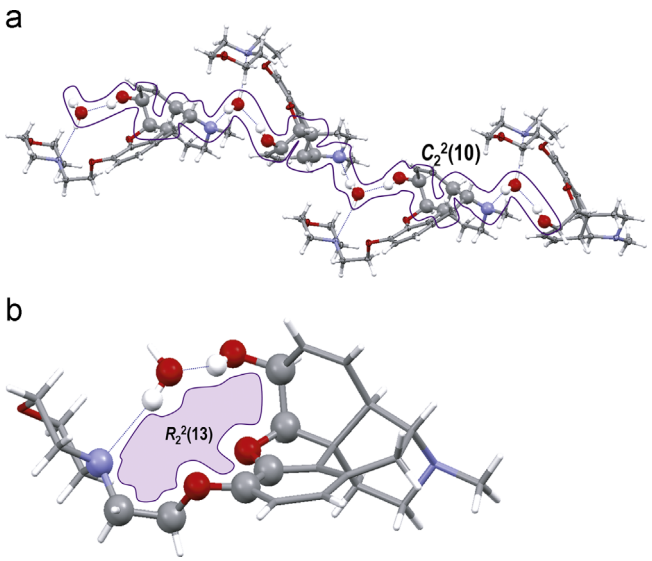

Fig. 6. Drawing of (a) an infinite helix *via* *y*-axis constituted of 10-member chains and (b) a 10-member ring formed by O–H···O and O–H···N–H-bonding described with corresponding *graph-set* descriptors.

differences (Fig. 3, Table. S2) both in the position and the shape of the observed single endotherm below 105 °C.

The observed endotherm on the DSC curves originates from the crystalline water evaporation and melting of pholcodine [21]. The observation is strongly supported by the TG/DTG data (Fig. S4), where up to 120 °C single mass loss step is observed. According to the obtained mass loses (Table. S2), varying from 3.90% up to 4.87% (4.43% for the commercial sample), the samples retained one water molecular equivalent after crystallization. The samples underwent total thermal degradation at temperature above 240 °C (Fig. S4).

The changes in the appearance of the melting/evaporation endotherm in the DSC curves (Fig. 3, Table. S2) are most probably governed by the different particle sizes and morphology (Fig. S1) of the crystals obtained in the various crystallization media. The samples were not ground before analysis to avoid influence on the structural preferences. Thus, the smaller crystals have better adhesion to the aluminum pan bottom than the larger ones, leading to differences manifested as apparent shift of the studied endotherm. In addition, the arbitrary orientation of microcrystals in the bulk causes differences in the empty space volume, influencing the proper heat distribution in the sample pan. One should also consider the possibility of low level impurities formation during the crystallization of the samples, which could additionally exert an influence over the melting/evaporation endotherm shape and position.

The cyclic DSC analysis (Fig. S1) revealed that, when cooled from 120 °C to 0 °C, all melted pholcodine samples (commercial and crystallized) did not crystallize upon cooling, and most probably remained amorphous. The result was confirmed by the second heating run, where in the range of 15 °C (commercial sample) up to 33 °C (ethanol crystallized sample), glass transition was registered. The changes in the temperature of glass transition are caused by the induced thermal history of the sample during the first heating and cooling runs.

3.1.3. *X-ray powder diffraction (XRPD)*

The XRPD patterns for the commercial sample of pholcodine monohydrate and the corresponding crystallized samples are presented in Fig. 4. Samples exhibit identical diffraction patterns confirming one crystalline form of pholcodine monohydrate. The XRPD results complement to the observed FT-IR spectroscopy findings proved that the observed DSC curve differences are due to instrumental factors and the sample preparation process.

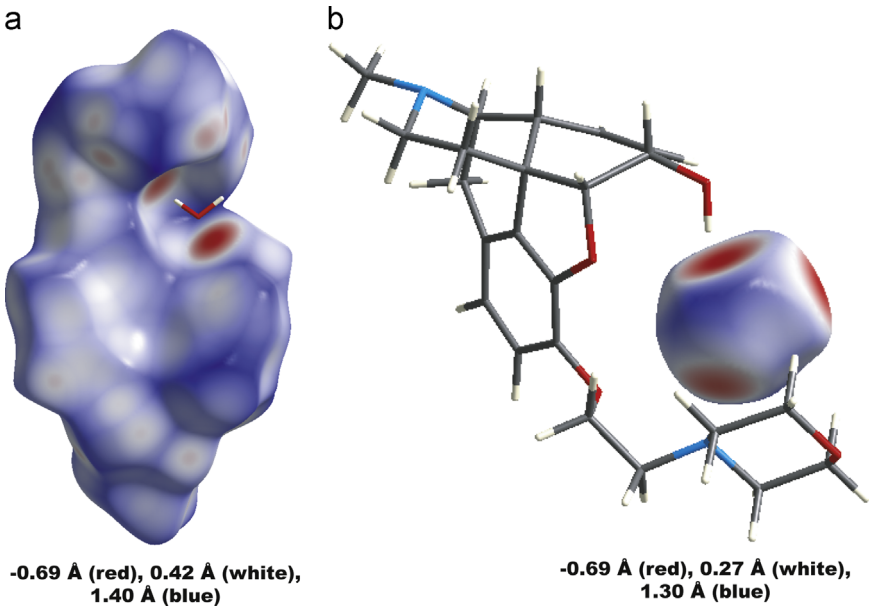

Fig. 7. View of the d_{norm} mapped on the Hirshfeld surface of (a) a pholcodine molecule and (b) a water molecule where the red color represents the area on the surface where the atoms make intermolecular contacts closer than the sum of their van der Waals radii. (For interpretation of the references to color in this figure legend, the reader is referred to the web version of this article.)

3.2. Single crystal X-ray diffraction analysis

3.2.1. Molecular structure

The convenient way to describe the molecular structure of pholcodine monohydrate is with reference to its rings. The molecule of pholcodine is constituted of 5 rings; the C1-to-C6 aromatic ring, the oxolanic O3–C2–C3–C7–C8 ring, the morpholinic N1–C19–C20–O1–C21–C22 ring and the methyl-piperidinic C7–C12–C13–N2–C16–C15 ring with the methyl group in equatorial position are in the chair conformation. The cyclohexenolic C7-to-C12 ring is in a boat conformation with the OH group in the equatorial position. ORTEP-3 drawing of the pholcodine monohydrate showing the crystallographic labeling scheme is shown in Fig. 5.

The Flack parameter and the absolute configuration of the compound cannot be undoubtedly determined because of the source of X-rays used (Mo) and the molecular formula (no atom heavier than O).

3.2.2. Crystal structure

Pholcodine monohydrate crystallizes in orthorhombic system in the space group $P2_12_12_1$. Each H_2O molecule is bonded to two molecules of pholcodine *via* three strong hydrogen bonds (Table 1). Molecules of pholcodine monohydrate form an infinite 1D helix parallel to the crystal *y*-axis (Fig. 6a) through strong O4–H4···O5w and O5w–H52w···N2^{i} hydrogen-bonds and moderate O5w–H51w···N1 H-bond. Corresponding *graph-set* motif is $C_2^2(10)$ for the 1D helix as can be seen in Fig. 6a. $R_2^2(13)$ *graph-set* descriptor can be assigned to the ring that is formed by H-bonding *via* O4–H4···O5w and O5w–H52w···N1 hydrogen bonds (Fig. 6b) [22]. The helices are interconnected via three very weak C–H···O hydrogen-bonds (Table 1). All other contacts are longer than 3.5 Å (sum of van der Waals radii). The packing diagram is shown in Fig. S6.

CCDC 910340 contains the relevant crystallographic data regarding the crystal structure of pholcodine monohydrate. Data can be obtained free of charge from the Cambridge Crystallographic Data Centre [26].

3.2.3. Hirshfeld surfaces

The visualization of the Hirshfeld three-dimensional d_{norm} surface [23–25] of the pholcodine molecule (Fig. 7a) reveals numerous interactions slightly stronger than van der Waals interactions (light red to white). However, there are two intensive red hot spots on the d_{norm} surface of a pholcodine molecule that correspond to two interactions with the water molecule. On the other hand, the d_{norm} surface of a water molecule has three red hot spots that correspond to interactions with two pholcodine molecules (Fig. 7b).

Partial fingerprint plots (Fig. S7c–g) of both pholcodine and water molecule show predominant O···H interactions (18% and 37%, respectively) followed by C···H interactions (9%) in pholcodine molecule. N···H interactions participate in overall interactions with 2% in pholcodine and with 16% in water molecule, respectively.

4. Conclusions

The crystallization of the commercial sample of pholcodine monohydrate from various organic solvents enabled growth of different size crystals with similar micro-morphology. The solvatomorphism study revealed one crystal modification of pholcodine monohydrate. It was concluded that the changes observed in the DSC traces of the studied materials are due to instrumental and sample preparation limitations, without exact physical relevance. Herein, the crystal structure of the pholcodine monohydrate, reported to the best of our knowledge for the first time, revealed that each water is connected to two pholcodine molecules *via* three strong hydrogen bonds. All other intermolecular H-bonds are not that strong what consequently affects the thermal properties of the compound. The water loss by means of heating is crucial and the compound melts afterwards at rather low temperature (less than 100 °C). The calculated XRPD pattern is in agreement with the corresponding experimental samples debyegrams obtained by recrystallization from six different solvents and title compound does not experience polymorphism under the applied study conditions. The presented data sheds light on the specific structural preferences of pholcodine monohydrate, being highly important regarding its physico-chemical stability when incorporated in various pharmaceutical dosage forms.

Acknowledgments

The authors would like to thank all the colleagues from the Research and Development department, ALKALOID AD-Skopje, for the support and the given useful suggestions during the preparation of this manuscript.

Appendix A. Supporting information

Supplementary data associated with this article can be found in the online version at http://dx.doi.org/10.1016/j.jcrysgro.2013.04.031.

References

[1] European Pharmacopoeia, Version 7.5, Monograph 0522, 2009 Edition.
[2] Z. Kovacs, S. Hosztafi, B. Noszal, Site specific acid-base properties of pholcodine and related compounds, Analytical and Bioanalytical Chemistry 386 (2006) 1709–1716.
[3] E. Florvaag, S.G.O. Johansson, The pholcodine story, Immunology and Allergy Clinics of North America 29 (2009) 419–427.
[4] J. Gore, B. Kasum, M.A. Holman, I.M. Scharfbiling, A.D. Ward, The structure of a human metabolite of pholcodine, Australian Journal of Chemistry 49 (1996) 1235–1242.
[5] M. Jairaj, D.G. Watson, M.H. Grant, A.I. Gray, G.G. Skellern, Comparative bitransformation of morphine, codeine and pholcodine in rat hepatocytes: identification of a novel metabolite of pholcodine, Xenobiotica 32 (2002) 1093–1107.
[6] O.M. Denk, A.I. Gray, G.G. Skellern, D.G. Watson, Isolation and identification of three potential impurities of pholcodine bulk drug substance, Journal of Pharmacy and Pharmacology 52 (2000) 819–829.
[7] A. Petkovska, H. Babunovska, M. Stefova, Fast and selective HPLC-DAD method for determination of pholcodine and related substances, Macedonian Journal of Chemistry and Chemical Engineering 30 (2011) 139–150.
[8] G. Petruševski, P. Naumov, G. Jovanovski, G. Bogoeva-Gaceva, S.W. Ng, Solid-state forms of sodium valproate, active component of the anticonvulsant drug epilim, ChemMedChem 3 (2008) 1377–1386.
[9] G. Petruševski, P. Naumov, G. Jovanovski, S.W. Ng, Unprecedented sodium–oxygen clusters in the solid-state structure of trisodiumhydrogentetravalproate monohydrate: a model for the physiological activity of the anticonvulsant drug Epilim, Inorganic Chemistry Communications 11 (2008) 81–84.
[10] G. Petruševski, S. Ugarkovic, P. Makreski, Solid-state transformation of the pseudopolymorphic forms of codeine phosphate hemihydrate and codeine phosphate sesquihydrate monitored by vibrational spectroscopy and thermal analysis, Journal of Molecular Structure 993 (2011) 328–335.
[11] G. Petruševski, M. Kajdžanoska, S. Ugarkovic, I. Micovski, G. Bogoeva-Gaceva, G. Jovanovski, P. Makreski, Solvatomorphism of codeine phosphate sesquihydrate – Vibrational spectroscopy and thermoanalytical characterization, Vibrational Spectroscopy 63 (2012) 460–468.
[12] Varian Resolution Pro software, Agilent Technologies, Inc., 2010–2011.
[13] Oxford Diffraction, Oxford Diffraction Ltd., Xcalibur CCD system, Crysalis CCD and CrysAlis RED software, Version 1.170, 2003.
[14] G.M Sheldrick, A short history of SHELX, Acta Crystallographica A64 (2008) 112–122.
[15] L.J. Farrugia, GX Win, Journal of Applied Crystallography 32 (1999) 837–838.
[16] L.J. Farrugia, ORTEP-3 for Windows, Journal of Applied Crystallography 30 (1997) 565–566.
[17] Persistence of Vision Pty Persistence of Vision Raytracer (POV-RAY). Version 3.6, 2004 ⟨http://www.povray.org.download/⟩.
[18] C.F. Macrae, I.J. Bruno, J.A. Chisholm, P.R. Edginton, P. McCabe, E. Pidcock, L. Rodriguez-Monge, R. Taylor, J.V.D. Streek, P.A. Wood, Mercury CSD 2.0 - New Features for the Visualization and Investigation of Crystal Structures, Journal of Applied Crystallography 41 (2008) 466–470.
[19] M.A. Spackman, D. Jayatilaka, Hirshfeld surface analysis, CrystEngComm 11 (2009) 19–32.
[20] M.A. Spackman, J.J. McKinnon, Fingerprinting intermolecular interactions in molecular crystals, CrystEngComm 4 (2002) 378–392.
[21] A.C. Moffat, M.D. Osselton, B. Widdop, Clarke's Analysis of Drugs and Poisons, third ed., Pharmaceutical Press, London, 2004.
[22] J. Bernstein, R.E. Davis, L. Shimoni, N.L. Chang, Patterns in hydrogen bonding: funcitonality and graph set analysis in crystals, Angewandte Chemie International Edition in English 34 (1995) 1555–1573.
[23] J.J. McKinnon, M.A. Spackman, A.S. Mitchell, Novel tools for visualizing and exploring intermolecular interactions in molecular crystls, Acta Crystallographica B60 (2004) 627–668.
[24] J.J. McKinnon, D. Jayatilaka, M.A. Spackman, Towards quantitative analysis of intermolecular interactions with Hirshfeld surfaces, Chemical Communications 37 (2007) 3814–3816.
[25] F.L. Hirshfeld, Bonded-atom fragments for describing molecular charge densities, Theoretica Chimica Acta 44 (1977) 129–138.
[26] ⟨www.ccdc.cam.ac.uk/data_request/cif⟩.